Published in final edited form as:

Chem Commun (Camb). 2020 August 18; 56(64): 9098–9101. doi:10.1039/d0cc03994b.

Quantifying the Effects of Quadrupolar Sink via ^{15}N Relaxation Dynamics in Metronidazoles Hyperpolarized via SABRE-SHEATH

Jonathan R. Birchall[a], **Mohammad S. H. Kabir**[a], **Oleg G. Salnikov**[b,c,d], **Nikita V. Chukanov**[b,c], **Alexandra Svyatova**[b,c], **Kirill V. Kovtunov**[b,c], **Igor V. Koptyug**[b,c], **Juri G. Gelovani**[a,e], **Boyd M. Goodson**[f], **Wellington Pham**[g], **Eduard Y. Chekmenev**[a,h]

[a]Department of Chemistry, Integrative Biosciences (Ibio), Wayne State University, Karmanos Cancer Institute (KCI), Detroit, Michigan 48202, United States.

[b]International Tomography Center, SB RAS, 3A Institutskaya St., Novosibirsk 630090, Russia

[c]Novosibirsk State University, 2 Pirogova St., Novosibirsk 630090, Russia

[d]Boreskov Institute of Catalysis SB RAS, 5 Acad. Lavrentiev Pr., Novosibirsk 630090, Russia

[e]United Arab Emirates University, Al Ain, United Arab Emirates

[f]Department of Chemistry and Biochemistry and Materials Technology Center, Southern Illinois University, Carbondale, Illinois 62901, United States

[g]Vanderbilt University Institute of Imaging Science (VUIIS), Department of Radiology, Vanderbilt University Medical Center (VUMC), Department of Biomedical Engineering, Vanderbilt University, Vanderbilt-Ingram Cancer Center (VICC), Nashville, Tennessee 37232-2310, United States

[h]Russian Academy of Sciences, Leninskiy Prospekt 14, Moscow, 119991, Russia

Abstract

^{15}N spin-lattice relaxation dynamics in metronidazole-$^{15}N_3$ and metronidazole-$^{15}N_2$ isotopologues are studied for rational design of ^{15}N-enriched biomolecules for Signal Amplification by Reversible Exchange in microtesla fields. ^{15}N relaxation dynamics mapping reveals the deleterious effects of interactions with polarization transfer catalyst and quadrupolar ^{14}N nucleus within the spin-relayed ^{15}N-^{15}N network.

Graphical Abstract

chekmenevlab@gmail.com.

†To the memory of Dr. Kirill V. Kovtunov (PhD, 1983–2020), friend, colleague, and mentor.

Electronic Supplementary Information (ESI) available: Numerical values of ^{15}N polarization build-up and polarization decay constants, additional experimental details (file type, PDF). See DOI: 10.1039/x0xx00000x

Conflicts of interest

BMG, EYC declare stake ownership in XeUS Technologies, LTD.

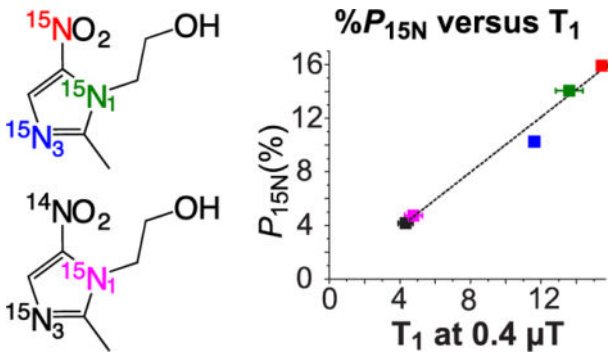

Presence of ^{14}N nucleus in the scalar coupling network causes deleterious effects in SABRE hyperpolarization in microtesla fields resulting in 3-fold decrease of ^{15}N T_1 and polarization values for all ^{15}N sites in $^{15}N_2$-isotopologue versus $^{15}N_3$-isotopologue.

The nuclear spin polarization P at thermal equilibrium is governed by a Boltzmann distribution of nuclear spins among Zeeman energy levels. P increases linearly with magnetic field strength. For a conventional high-field NMR spectrometer (*e.g.*, 9.4 T) or clinical Magnetic Resonance Imaging (MRI) scanner (*e.g.*, 3 T) at room temperature, P is typically on the order of 10^{-5} to 10^{-6}, resulting in a relatively low sensitivity of NMR-based applications. For NMR applications where this sensitivity is too low to be useful, various hyperpolarization strategies may be employed to increase P by as much as 4–5 orders of magnitude,[1, 2] with corresponding signal gains.

One such technique is Signal Amplification by Reversible Exchange (SABRE), pioneered by Duckett *et al.* in 2009,[3] which utilizes simultaneous reversible chemical exchange of parahydrogen (p-H_2) and to-be-hyperpolarized substrate molecules at a metal center. In SABRE, the transfer of nuclear spin polarization from parahydrogen-derived hydrides to a spin-polarizable substrate occurs spontaneously via the network of spin-spin couplings established in a transient polarization transfer catalyst (PTC) complex (Figure 1a).[3–5] While several approaches have been developed for polarization transfer in SABRE,[6–11] a variant of SABRE, SABRE-SHEATH (SABRE in SHield Enables Alignment Transfer to Heteronuclei),[12, 13] facilitates the generation of highly polarized spin states of heteronuclei[14–17] including nitrogen-15 with high polarization (P_{15N}>30%[18]) persisting for tens of minutes.[19] Nitrogen is found in a wide range of biomolecules including nucleic acids, amino acids, proteins, and drugs. Since SABRE-SHEATH is performed at very low magnetic fields (< 1 μT) and near room temperature, the production of such HP ^{15}N spin-labeled biomolecules is comparatively simple, fast and inexpensive.[10]

Nitroimidazoles can be readily reduced in anaerobic environments. This property has been widely employed in a number of antibiotic drugs,[20] Positron Emission Tomography (PET) tracers for hypoxia sensing,[21] and also in a number of emerging cancer therapeutics: *e.g.*, evofosfamide (a.k.a. TH-302)[22] and the radiosensitizer nimorazole.[23]

Metronidazole is an FDA-approved antibiotic,[24] belonging to the nitroimidazole class of compounds. We envision that ^{15}N-hyperpolarized metronidazole can be potentially

employed for hypoxia sensing in a manner similar to that of nitroimidazole-based Positron Emission Tomography (PET) tracers. One such tracer, ^{18}F-fluoromisonidazole (FMISO),[21] undergoes reduction in hypoxic environment (including most notably hypoxic tumors) and the metabolic products of this reduction process become trapped in hypoxic cells, providing contrast in FMISO PET images.[25] The enormous potential for using HP MRI to sense metabolic transformations *in vivo* has been well demonstrated[10, 26]; correspondingly, HP MRI of metronidazole may obviate the limitations of FMISO PET imaging, including the use of ionizing radiation, the requirement for long clearance time from surrounding tissues, and the inability to spectrally distinguish parent compounds from downstream products.

We have demonstrated efficient SABRE-SHEATH hyperpolarization of the $^{15}N_3$ site in natural abundance metronidazole with $\%P_{15N}$ exceeding 30%.[18] This nitrogen site directly interacts with the PTC, and therefore gains its polarization directly from p-H_2-derived hydrides. Subsequently, commercially available metronidazole-$^{15}N_2$-$^{13}C_2$ (Sigma-Aldrich, #32744) was employed for SABRE-SHEATH, but unfortunately yielded significantly lower $\%P_{15N}$ (roughly by an order of magnitude), although all ^{15}N- and ^{13}C-labeled sites have been successfully hyperpolarized.[27, 28] Most recently we have synthesized metronidazole-$^{15}N_3$ and demonstrated $^{15}N \rightarrow {}^{15}N$ spin-relayed SABRE-SHEATH hyperpolarization via two-bond ^{15}N-^{15}N spin-spin couplings, Figure 1d. This metronidazole-$^{15}N_3$ isotopologue exhibited a remarkable $\%P_{15N}$ of ~16% on all three ^{15}N sites including $^{15}NO_2$, which has a polarization relaxation decay constant T_1 approaching 10 minutes. However, in order to facilitate more effective production of HP biomolecules for bioimaging applications, it is clearly necessary to gain improved understanding of the underlying spin-relaxation phenomena to inform the rational design of these promising imaging agents.

Here, we report a quantitative study of spin relaxation dynamics of metronidazole-$^{15}N_2$ and metronidazole-$^{15}N_3$ isotopologues, Figure 1c and Figure 1d respectively, using previously described experimental setup (Figure S2).[27, 29] Catalyst activation was performed for approximately 2 h for each sample studied to ensure reproducibility, see Figure S1 in the Supporting Information (SI). Other experimental parameters (temperature, p-H_2 pressure, flow rate and in-shield magnetic field) were optimized for each isotopologue, Figure S1. Using an overpressure of 94 psig, p-H_2 was bubbled through a solution of MNZ ^{15}N-isotopologue substrate and Ir-IMes catalyst in 0.6 mL methanol-d_4 for one minute to facilitate polarization transfer in microtesla fields. Following polarization build-up, the sample solution was rapidly transferred (2–4 s to minimize the relaxation losses) to a 1.4 T NMR Pro (Nanalysis, Canada) bench-top NMR spectrometer for ^{15}N NMR detection (Figure 1h). Each relaxation/build-up curve was obtained by varying the time duration that the sample spent in a given magnetic field.

The key results related to ^{15}N T_1 relaxation at the optimal magnetic field during the SABRE-SHEATH polarization transfer process (*ca.* 0.4 μT, Figure S1) for metronidazole-$^{15}N_3$ and metronidazole-$^{15}N_2$ are shown in Figures 2e and 2f, respectively. As expected for microtesla magnetic fields, all ^{15}N sites within a given molecule share approximately the same relaxation rate (*e.g.*, 13.8–15.4 s for MNZ-$^{15}N_3$, Figure 2e). However, the $^{15}NO_2$ group replacement by $^{14}NO_2$ leads to dramatic, 3-fold shortening of the

^{15}N T_1 (4.3–4.8 s corresponding T_1 values for MNZ-$^{15}N_2$, Figure 2f). This striking effect can be explained by the enhanced scalar relaxation of the second kind[30, 31] induced by the quadrupolar $^{14}NO_2$ site within the N-N spin-spin coupling network. These results are further supported by the overall similar ^{15}N T_1 trend at the Earth's magnetic field (*ca.* 10 μT in the basement of our lab at Detroit, MI, Table S1). Moreover, we find that each ^{15}N polarization build-up constant (T_b, Figure 2c and Figure 2d) at 0.4 μT is closely correlated with the corresponding T_1 value. In practice, this means that the increased relaxation rate caused by the presence of the quadrupolar ^{14}N spin in MNZ-$^{15}N_2$ (despite the peripheral position of the NO_2 group) allows for achieving the steady-state $\%P_{15N}$ faster on $^{15}N_3$ and $^{15}N_1$ sites—but at significantly lower levels. The correlation plot of $\%P_{15N}$ versus T_1 at 0.4 μT indeed exhibits a linear trend with R^2>0.99 (Figure 2inset). When the magnetic field is sufficiently high (*e.g.*, 1.4 T, Figure 2g and Figure 2h), the increased frequency dispersion of the nuclear spins puts them in a weakly coupled regime with ^{15}N sites having significantly longer T_1 decay constants—on the order of many minutes.

On another note, the realization that scalar-coupled ^{14}N spins are highly deleterious in the context of SABRE-SHEATH suggests that if these quadrupolar effects would have been avoided, near-unity P_{15N} would have been potentially achievable in the previous studies.[18]

It should be pointed out that substrate exchange of Ir-IMes catalyst may act as the potential source of additional undesirable ^{15}N relaxation (*e.g.*, due to compounding effects of quadrupolar Ir nucleus and the chemical exchange process).[13] Consequently, a series of control experiments were performed, where the catalyst concentration was systematically varied from 0.5 mM to 1 mM to 2 mM at a fixed concentration of metronidazole isotopologue (Figures S3a–d). The [catalyst] increase from 0.5 mM to 2 mM results in a stepwise decrease in ^{15}N T_1 and T_b by approximately 2-fold at 0.4 μT (Figure S3b and Figure S3c). However, because the interplay of T_1 relaxation and catalyst concentration is complex in the SABRE process,[32, 33] these decreases in ^{15}N T_1 and T_b at 0.4 μT are offset by the overall increased catalyst-to-substrate ratio (*i.e.*, better substrate access to p-H_2 spin bath), resulting in somewhat greater $\%P_{15N}$ in metronidazole-$^{15}N_3$ and similar $\%P_{15N}$ in metronidazole-$^{15}N_2$ at higher [catalyst], Figure S3d. Of note, the Ir-IMes catalyst decreases ^{15}N T_1 even at high magnetic fields (1.4 T, weakly coupled regime) for $^{15}NO_2$ (Figure S3a). Moreover, this observation clearly indicates a second reason (beyond agent purification) that SABRE catalyst removal[18, 34–36] is warranted as soon polarization build-up is completed to minimize ^{15}N polarization losses prior to biomedical utilization of HP metronidazole-$^{15}N_3$ as a contrast agent.

The high levels of ^{15}N polarization obtained in ^{15}N-labeled metronidazole isotopologues enable direct ^{15}N MRI. Figure 3 demonstrates the 2D ^{15}N projection images of 5 mm NMR tubes filled with HP solutions of ^{15}N-labeled metronidazole isotopologues with the highest spatial resolution reported to date to the best of our knowledge.

Conclusions

In summary, the spin-relayed SABRE-SHEATH hyperpolarization approach allows efficient polarization of scalar coupled ^{15}N-^{15}N spin networks. These networks may be created via

two-bond ^{15}N-^{15}N J-couplings at most. The presence of ^{14}N spins in such networks must be avoided to prevent deleterious polarization losses due to quadrupolar relaxation effects (manifested on ^{15}N as scalar relaxation of the second kind[16]), in order to maximize the resulting $\%P_{15N}$. Although the catalyst decreases the ^{15}N spin-relaxation time constant, T_1, of metronidazole isotopologues in the microtesla regime in a concentration-dependent manner, the overall impact on the achievable ^{15}N polarization level is relatively minor. On the other hand, the presence of a ^{14}N nucleus in the scalar coupling network results in an approximately 3-fold decrease of microtesla ^{15}N T_1 values for all ^{15}N sites in the $^{15}N_2$-isotopologue versus the $^{15}N_3$-isotopologue over a wide range of catalyst concentrations. This ^{15}N T_1 reduction results in a corresponding 3-fold decrease of ^{15}N polarization levels. These findings have substantial translational relevance for the rational design of hyperpolarized MRI contrast agents comprising ^{15}N- and ^{13}C-labeled biomolecules—both in general, and in the specific case of SABRE-hyperpolarized metronidazole, an antibiotic that can be potentially employed for non-invasive hypoxia sensing antibiotics,[20] emerging cancer therapeutics such as evofosfamide[22] and nimorazole radiosensitizers,[23] etc. Feasibility of high resolution MRI of HP metronidazole is shown, which bodes well for potential biomedical applications.

Supplementary Material

Refer to Web version on PubMed Central for supplementary material.

Acknowledgements

This work was supported by the NSF under grants CHE-1904780 and CHE-1905341, NIH R21CA220137, DOD CDMRP W81XWH-12-1-0159/BC112431, W81XWH-15-1-0271 and W81XWH-15-1-0272. O.G.S. thanks the RFBR (#19-33-60045) for the support of mechanistic studies with the use of parahydrogen. N.V.C. and K.V.K. thank the RFBR and Novosibirsk region government (#18-43-543023) for their support in the synthesis of ^{15}N-labeled compounds. I.V.K. thanks the Russian Ministry of Science and Higher Education (project AAAA-A16-116121510087-5) and the RFBR (#19-29-10003, #17-54-33037) for financial support.

Notes and References

1. Ardenkjaer-Larsen JH, J. Magn. Reson, 2016, 264, 3–12. [PubMed: 26920825]
2. Kovtunov KV, Pokochueva EV, Salnikov OG, Cousin S, Kurzbach D, Vuichoud B, Jannin S, Chekmenev EY, Goodson BM, Barskiy DA and Koptyug IV, Chem. Asian J, 2018, 13, 1857–1871.
3. Adams RW, Aguilar JA, Atkinson KD, Cowley MJ, Elliott PIP, Duckett SB, Green GGR, Khazal IG, Lopez-Serrano J and Williamson DC, Science, 2009, 323, 1708–1711. [PubMed: 19325111]
4. Rayner PJ and Duckett SB, Angew. Chem. Int. Ed, 2018, 57, 6742–6753.
5. Cowley MJ, Adams RW, Atkinson KD, Cockett MCR, Duckett SB, Green GGR, Lohman JAB, Kerssebaum R, Kilgour D and Mewis RE, J. Am. Chem. Soc, 2011, 133, 6134–6137. [PubMed: 21469642]
6. Green RA, Adams RW, Duckett SB, Mewis RE, Williamson DC and Green GGR, Prog. Nucl. Mag. Res. Spectrosc, 2012, 67, 1–48.
7. Ivanov KL, Pravdivtsev AN, Yurkovskaya AV, Vieth H-M and Kaptein R, Prog. Nucl. Mag. Res. Spectrosc, 2014, 81, 1–36.
8. Pravdivtsev AN, Yurkovskaya AV, Zimmermann H, Vieth H-M and Ivanov KL, RSC Adv, 2015, 5, 63615–63623.
9. Pravdivtsev AN, Yurkovskaya AV, Vieth H-M and Ivanov KL, J. Phys. Chem. B, 2015, 119, 13619–13629. [PubMed: 25970807]

10. Hövener J-B, Pravdivtsev AN, Kidd B, Bowers CR, Glöggler S, Kovtunov KV, Plaumann M, Katz-Brull R, Buckenmaier K, Jerschow A, Reineri F, Theis T, Shchepin RV, Wagner S, Bhattacharya P, Zacharias NM and Chekmenev EY, Angew. Chem. Int. Ed, 2018, 57, 11140–11162.
11. Barskiy DA, Kovtunov KV, Koptyug IV, He P, Groome KA, Best QA, Shi F, Goodson BM, Shchepin RV, Truong ML, Coffey AM, Waddell KW and Chekmenev EY, ChemPhysChem, 2014, 15, 4100–4107. [PubMed: 25367202]
12. Theis T, Truong ML, Coffey AM, Shchepin RV, Waddell KW, Shi F, Goodson BM, Warren WS and Chekmenev EY, J. Am. Chem. Soc, 2015, 137, 1404–1407. [PubMed: 25583142]
13. Truong ML, Theis T, Coffey AM, Shchepin RV, Waddell KW, Shi F, Goodson BM, Warren WS and Chekmenev EY, J. Phys. Chem. C, 2015, 119, 8786–8797.
14. Duckett S, Roy S, Norcott P, Rayner PJ and Green GGR, Chem. Eur. J, 2017, 23, 10496–10500. [PubMed: 28627764]
15. Olaru AM, Robertson TBR, Lewis JS, Antony A, Iali W, Mewis RE and Duckett SB, ChemistryOpen, 2018, 7, 97–105. [PubMed: 29318102]
16. Barskiy DA, Shchepin RV, Tanner CPN, Colell JFP, Goodson BM, Theis T, Warren WS and Chekmenev EY, ChemPhysChem, 2017, 18, 1493–1498. [PubMed: 28517362]
17. Shchepin RV, Goodson BM, Theis T, Warren WS and Chekmenev EY, ChemPhysChem, 2017, 18, 1961–1965. [PubMed: 28557156]
18. Kidd BE, Gesiorski JL, Gemeinhardt ME, Shchepin RV, Kovtunov KV, Koptyug IV, Chekmenev EY and Goodson BM, J. Phys. Chem. C, 2018, 122, 16848–16852.
19. Shchepin RV, Birchall JR, Chukanov NV, Kovtunov KV, Koptyug IV, Theis T, Warren WS, Gelovani JG, Goodson BM, Shokouhi S, Rosen MS, Yen Y-F, Pham W and Chekmenev EY, Chem. Eur. J, 2019, 25, 8829–8836. [PubMed: 30964568]
20. Nepali K, Lee H-Y and Liou J-P, J. Med. Chem, 2018, 62, 2851–2893. [PubMed: 30295477]
21. Hendrickson K, Phillips M, Smith W, Peterson L, Krohn K and Rajendran J, Radiother. Oncol, 2011, 101, 369–375. [PubMed: 21872957]
22. O'Connor LJ, Cazares-Körner C, Saha J, Evans CNG, Stratford MRL, Hammond EM and Conway SJ, Org. Chem. Front, 2015, 2, 1026–1029.
23. ClinicalTrials.gov, Clinical tiral #NCT01507467.
24. Roy RB, Laird SM and Heasman L, Br. J. Vener. Dis, 1975, 51, 281–284. [PubMed: 1098732]
25. Masaki Y, Shimizu Y, Yoshioka T, Tanaka Y, Nishijima K.-i., Zhao S, Higashino K, Sakamoto S, Numata Y, Yamaguchi Y, Tamaki N and Kuge Y, Sci. Rep, 2015, 5, 16802. [PubMed: 26582591]
26. Kurhanewicz J, Vigneron DB, Brindle K, Chekmenev EY, Comment A, Cunningham CH, DeBerardinis RJ, Green GG, Leach MO, Rajan SS, Rizi RR, Ross BD, Warren WS and Malloy CR, Neoplasia, 2011, 13, 81–97. [PubMed: 21403835]
27. Shchepin RV, Jaigirdar L, Theis T, Warren WS, Goodson BM and Chekmenev EY, J. Phys. Chem. C, 2017, 121, 28425–28434.
28. Shchepin RV, Jaigirdar L and Chekmenev EY, J. Phys. Chem. C, 2018, 122, 4984–4996.
29. Theis T, Ariyasingha NM, Shchepin RV, Lindale JR, Warren WS and Chekmenev EY, J. Phys. Chem. Lett, 2018, 9, 6136–6142. [PubMed: 30284835]
30. Bernatowicz P, Kubica D, Ociepa M, Wodyński A and Gryff-Keller A, J. Phys. Chem. A, 2014, 118, 4063–4070. [PubMed: 24835107]
31. Blanchard JW, Sjolander TF, King JP, Ledbetter MP, Levine EH, Bajaj VS, Budker D and Pines A, Phys. Rev. B, 2015, 92, 220202.
32. Barskiy DA, Pravdivtsev AN, Ivanov KL, Kovtunov KV and Koptyug IV, Phys. Chem. Chem. Phys, 2016, 18, 89–93. [PubMed: 26645782]
33. Barskiy DA, Knecht S, Yurkovskaya AV and Ivanov KL, Prog. Nucl. Mag. Res. Spectrosc, 2019, 114-115, 33–70.-
34. Barskiy DA, Ke LA, Li X, Stevenson V, Widarman N, Zhang H, Truxal A and Pines A, J. Phys. Chem. Lett, 2018, 9, 2721–2724. [PubMed: 29739186]
35. Mewis RE, Fekete M, Green GGR, Whitwood AC and Duckett SB, Chem. Comm, 2015, 51, 9857–9859. [PubMed: 25989727]

36. Manoharan A, Rayner P, Iali W, Burns M, Perry V and Duckett S, ChemMedChem, 2018, 13, 352–359. [PubMed: 29232489]

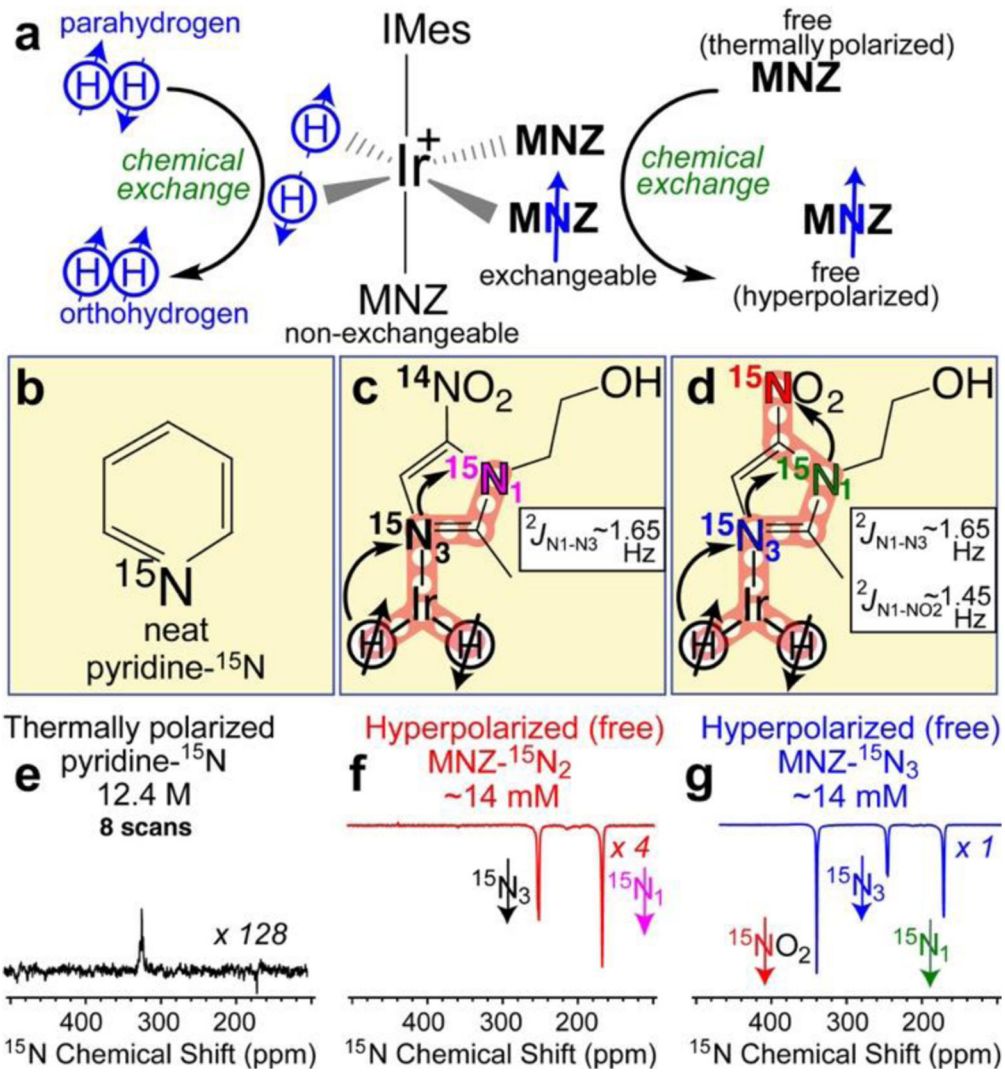

Figure 1.

a) Molecular exchange between p-H_2 and substrate, *e.g.*, metronidazole (MNZ) employed here, in SABRE hyperpolarization. b) Structure of pyridine-^{15}N employed as a signal reference. c-d) Corresponding structures and polarization transfer spin-relays (red overlay) between p-H_2 and ^{15}N nuclei in corresponding MNZ ^{15}N-isotopologues. e) Signal reference ^{15}N NMR spectrum of a thermally polarized neat pyridine-^{15}N acquired with 8 scans and 10-minute recovery time. f-g) Corresponding ^{15}N NMR spectra of HP metronidazole-$^{15}N_2$ and metronidazole-$^{15}N_3$.

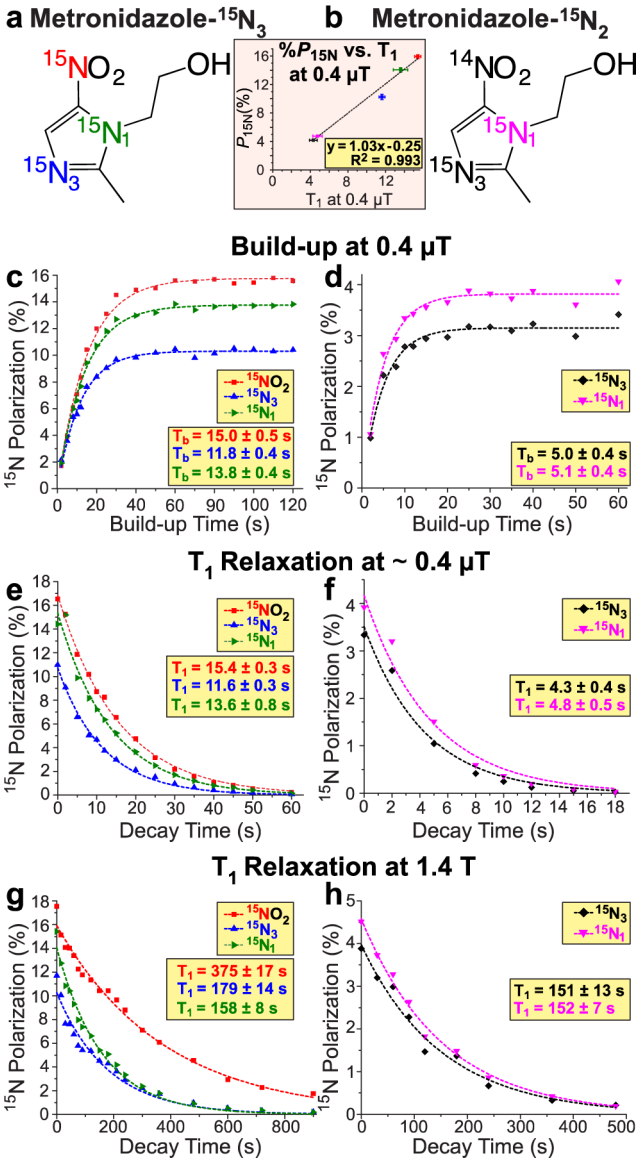

Figure 2.

a-b) Structures of two metronidazole ^{15}N-isotopologues. c-d) Corresponding ^{15}N polarization build-up curves at 0.4 µT. e-f) Corresponding ^{15}N T_1 decay curves at 0.4 µT. g-h) Corresponding ^{15}N T_1 decay curves at 1.4 T. The presented data was recorded using a 2 mM IrIMes catalyst concentration and a corresponding 20 mM MNZ isotopologue concentration. All experiments are performed in CD_3OD.

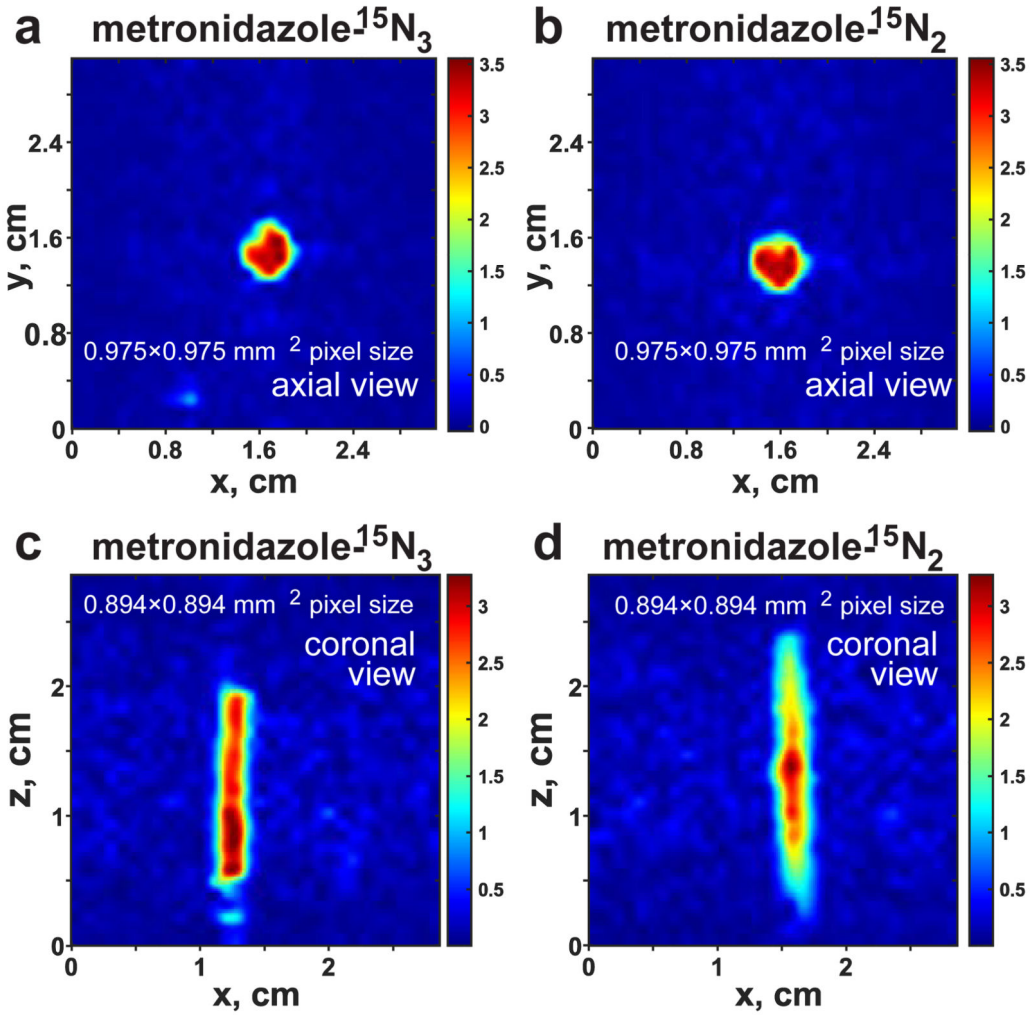

Figure 3.

^{15}N MRI of 5 mm NMR tubes filled with hyperpolarized solutions of 0.1 M metronidazole-$^{15}N_3$ (MNZ-$^{15}N_3$) and metronidazole-$^{15}N_2$ (MNZ-$^{15}N_2$) respectively using 5 mM of Ir(COD)(IMes)Cl in methanol-d_4 obtained by TrueFISP pulse sequence. Imaging parameters employed: TR = 62.5 ms, TE = 3.6 ms, scan time = 2.0 seconds, flip angle = 15˚, matrix size = 32×32 (zero-filled to 512×512). a) axial projection 2D image of metronidazole-$^{15}N_3$ using 1 average (maximum SNR(SNR_{MAX}) is ~500, b) axial projection 2D image of metronidazole-$^{15}N_2$ using 1 average, SNR_{MAX} is ~410, c) coronal projection 2D image of metronidazole-$^{15}N_3$ using 8 averages, SNR_{MAX} is ~450, d) coronal projection 2D image of metronidazole-$^{15}N_2$ using 8 averages, SNR_{MAX} is ~340.